Journal of Power Sources 249 (2014) 349–356

Contents lists available at ScienceDirect

Journal of Power Sources

journal homepage: www.elsevier.com/locate/jpowsour

Tortuosity characterization of 3D microstructure at nano-scale for energy storage and conversion materials

Yu-chen Karen Chen-Wiegart [a], Ross DeMike [b], Can Erdonmez [c], Katsuyo Thornton [b], Scott A. Barnett [d], Jun Wang [a,*]

[a] Photon Science Directorate, Brookhaven National Laboratory, 744 Ring Road, Upton, NY 11973, USA
[b] Department of Materials Science and Engineering, University of Michigan, 2300 Hayward St., Ann Arbor, MI 48109, USA
[c] Sustainable Energy Technologies Department, Brookhaven National Laboratory, 734 Brookhaven Ave., Upton, NY 11973, USA
[d] Department of Materials Science and Engineering, Northwestern University, 2220 Campus Drive, Evanston, IL 60208, USA

HIGHLIGHTS

- Fast 3D tortuosity calculation, critical for energy storage/conversion materials.
- Novel concept of path-dependent tortuosity distribution account for inhomogeneity.
- 3D nanostructure of lithium ion battery and solid oxide fuel cell were studied.
- The present method agree well with the effective diffusion-based tortuosity values.
- The method can be applied to any porous medium where diffusion is critical.

GRAPHICAL ABSTRACT

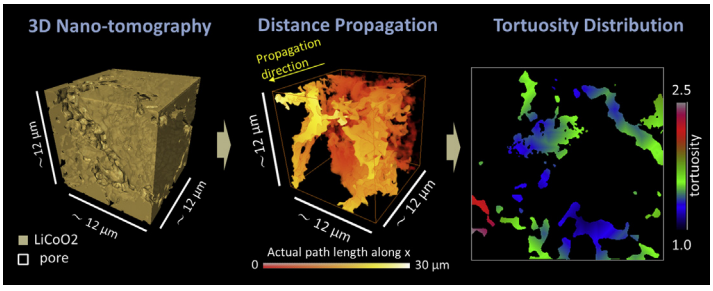

ARTICLE INFO

Article history:
Received 6 September 2013
Accepted 9 October 2013
Available online 30 October 2013

Keywords:
Lithium ion battery
Solid oxide fuel cell
Tortuosity
X-ray tomography
Three dimensional structure
Novel charaterization

ABSTRACT

A distance propagation method is presented for calculating tortuosity with relatively low computation time from three-dimensional (3D) tomographic data. Moreover, a novel concept of tortuosity distribution is developed to provide a more comprehensive picture of inhomogeneous microstructures where tortuosity depends on the actual 3D paths. Instead of using one single tortuosity value, the tortuosity distribution both as spatial distribution map and also statistic histogram can provide a more complete description. The method, which can be applied to any porous medium, is tested against a diffusion-based tortuosity calculation on two 3D microstructures: a LiCoO2 cathode electrode of lithium ion battery measured by x-ray nano-tomography and a lanthanum strontium manganite–yttria-stabilized zirconia, solid oxide fuel cells cathode measured using focused ion beam-scanning electron microscopy serial sectioning. The present method is shown to provide good-agreement with the effective diffusion-based tortuosity values.

1. Introduction

Tortuosity is an important parameter for characterizing transport properties of multi-phase structures, and is of interest in a broad range of fields such as energy storage and conversion materials [1–4], catalysts [5,6] and soil mechanisms [7–9]. Tortuosity,

* Corresponding author. Tel.: +1 631 344 2661; fax: +1 631 344 8189.
E-mail address: junwang@bnl.gov (J. Wang).

0378-7753/$ – see front matter © 2013 Elsevier B.V. All rights reserved.
http://dx.doi.org/10.1016/j.jpowsour.2013.10.026

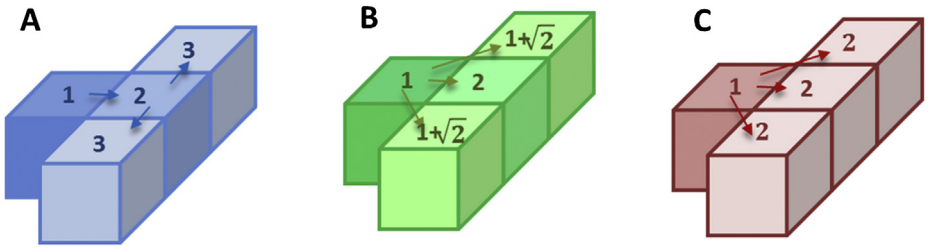

Fig. 1. Three different voxel neighboring definitions: (A) city-block, (B) quasi-Euclidean and (C) chess-board.

defined as the ratio between the actual tortuous path length to the straight-though path length, is the parameter that embodies how the specific phase structure influences transport. As three dimensional (3D) structural measurements have become increasingly available, it has become useful to calculate tortuosity values directly from measured 3D structures. One example is for characterizing, modeling, and designing energy storage and conversion materials such as batteries and fuel cells, where transport within the electrodes is directly relevant to electrochemical properties.

The importance of tortuosity for battery electrodes has been discussed previously [1,2,10–17]. Given that active electrode materials in Li-ion batteries make up typically 50–70% of electrode volume, and that the remaining volume is shared between electrolyte, binder, and carbon phases, Li-ion transport in the electrolyte phase may limit battery capacity, compared with the electronic conductivity and charge-transfer [18,19], in some cases. Attempts to increase the density of active materials or increase electrode thickness, in order to increase the energy density, will ultimately be limited by maintaining the ion transport [1]. Electrolyte-phase tortuosity is thus a key factor in design of electrodes. Advanced processing approaches have been used to design battery electrode morphology and architecture to improve power performance via minimizing the electrode tortuosity and therefore to maximize power with a given porosity and thickness of the electrodes [1]. In addition, others have used tortuosity as an effective geometric parameter in models to describe ionic transport in the porous electrode [2,12,20,21]. Similarly, the importance of tortuosity has also been discussed in many literature regarding energy conversion materials such as proton exchange membrane fuel cells and solid oxide fuel cells (SOFC) [3,4,22–27]. In SOFC electrodes, tortuosity of

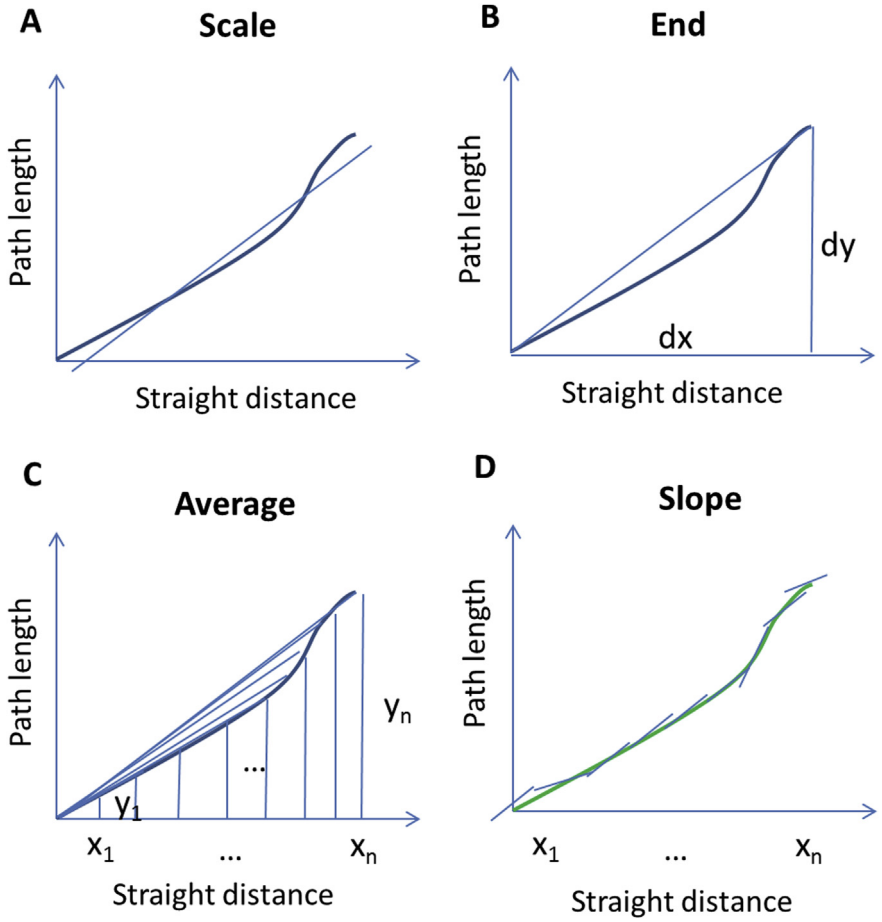

Fig. 2. Four different methods to extract the tortuosity from the distance curve. (A) Scale: the curve is fitted with: $y = mx + b$ where x is the straight distance, y is the path length and the tortuosity is m. (B) End: tortuosity is defined by average path length at the end plane divided by the straight distance. (C) Average: tortuosity is defined by the average tortuosity from each plane; tortuosity $= 1/n \sum_{i=1}^{n} \boldsymbol{y}_i/\boldsymbol{x}_i$. (D) Slope: tortuosity is extracted by average of all local slopes. The local slopes are obtained from first fitting the curve first with a polynomial with degree of five and then calculating the derivative at each x (straight distance) point.

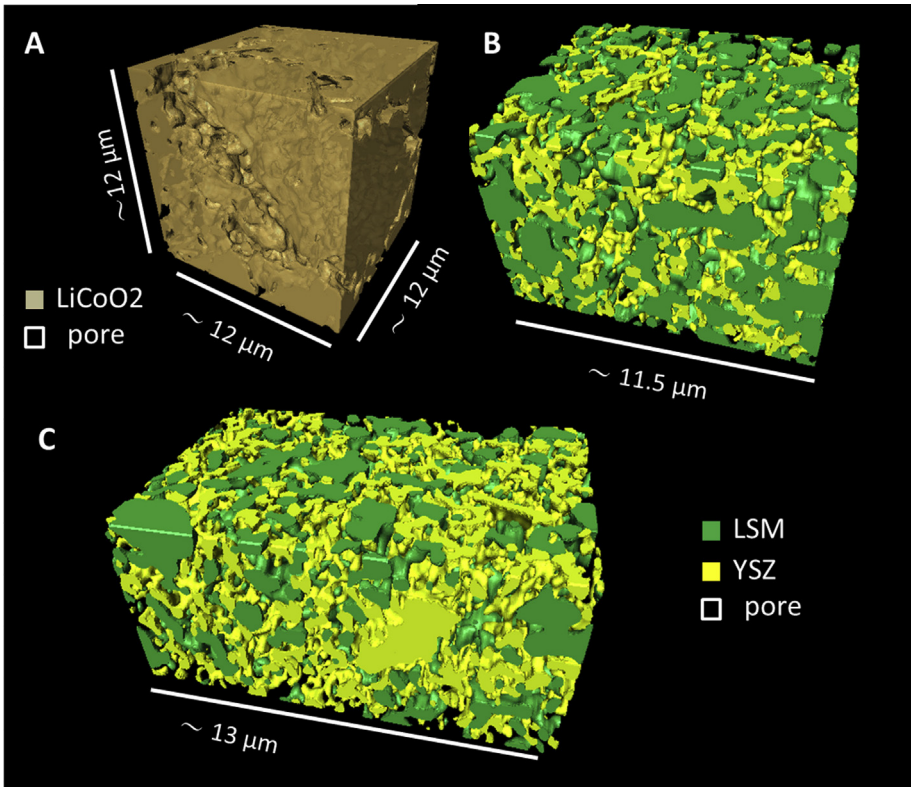

Fig. 3. Cropped reconstructed 3D structure of the (A) LiCoO2 sample imaged by x-ray nano-tomography. (B) 70/30 LSM–YSZ sample and (C) 50/50 LSM–YSZ samples imaged by FIB-SEM serial sectioning.

the pore and ionically-conducting phases may both be important. Vapor transport in the pore phase is directly related to concentration polarization [28], while oxygen ion transport in ionic-conductor phases can limit the effective active thickness in the electrode [29].

Two different types of tortuosity calculation have been reported previously. One is the effective diffusivity method, based on simulating the diffusive or conductive transport across one phase in a measured 3D microstructure; dividing by the transport flux for straight-through paths yields the tortuosity factor [10,23,30]. The other method is a geometrical calculation where the lengths of the tortuous paths in the 3D microstructures are measured; the resulting path length divided by the straight-through path length is the tortuosity [3,31]. Path length calculation has been done in various ways, including distance prorogation [32] and shortest path search [3]. While the geometrical method is computationally much less intensive compared with the effective diffusivity method, it is not clear how well the tortuosity calculated from geometrical methods represents the diffusion behavior. No direct comparison has been reported yet to address the difference or similarity between these methods. Furthermore, the prior calculations yield only one tortuosity value to represent inhomogeneous structures, and hence do not provide information on the tortuosity variation within the structure [3,33–36].

Here we describe a path-length method to characterize the tortuosity of phases in various complex 3D microstructures, and compare the resulting values with effective diffusivity method calculations on the same microstructures. We further developed a concept of tortuosity distribution by visualizing a spatial distribution of the tortuosity, and also quantifying the tortuosity variation with histograms to overcome this major drawback. Various microstructures with a range of structural characteristics and tortuosity values are considered.

2. Method

2.1. Background

Tortuosity is defined as the ratio between the actual path length to the straight distance. For a porous medium with L_{eff} as the effective actual path length from point A to point B, and the L as the straight distance (Euclidean distance), the strict geometrical definition of its tortuosity (τ) is:

$$\tau = \frac{L_{\text{eff}}}{L}. \tag{1}$$

Geometrical method directly uses this definition to calculate tortuosity by measuring L_{eff} and L.

Historically, this geometry factor was introduced by solving the one-dimensional diffusion problem, Fick's first law of diffusion:

$$J = -D\frac{\partial c}{\partial x}, \tag{2}$$

where J is the flux of diffusing species, D is its diffusion coefficient, c is its concentration and x is the position along the diffusion path. To relate diffusion in porous media to equation (2), it was assumed that the transport media are cylindrical capillaries [37]. This leads to the relationship between the diffusion coefficient D in a non-tortuous path and the effective diffusion coefficient D_{eff} in a tortuous path:

$$D_{\text{eff}} = D\frac{\varepsilon}{\left(\frac{L_{\text{eff}}}{L}\right)^2} = D\frac{\varepsilon}{\tau^2}, \tag{3}$$

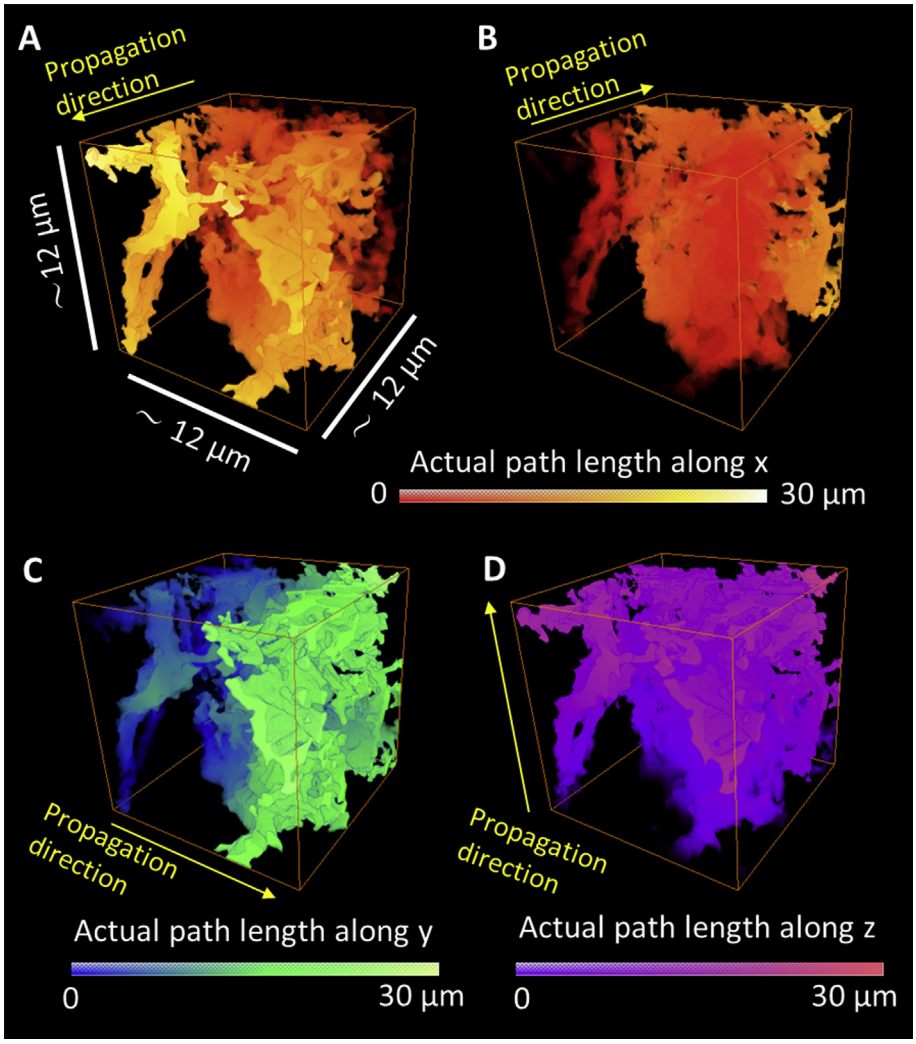

Fig. 4. Three-dimensional (3D) distance map based on geometric prorogation. The neighboring definition used here in the figure is city-block. (A) propagating along positive *x* direction, (B) propagating along negative *x* direction, (C) propagating along positive *y* direction and (D) propagating along positive *z* direction. The 3D distance maps for the negative *y* and *z* directions are not shown here for brevity.

where ε is the volume fraction of the pores. The geometry factor tortuosity (τ) was then defined as L_{eff}/L shown in equation (1). The square of tortuosity is therefore called tortuosity factor (T), defined as:

$$T = \left(\frac{L_{\text{eff}}}{L}\right)^2 = \tau^2. \quad (4)$$

Though it is common to see the mix use of the tortuosity (τ) and the tortuosity factor (T) in the literature, extra caution should be taken to avoid this confusion. Tortuosity calculation based on effective diffusivity method can then be performed using equation (3) or its equivalent.

2.2. Approach

In this paper, both Li-ion battery and SOFC electrode structures were used to test the accuracy of the present calculation. First, a porous $LiCoO_2$ structure, cathode electrode of Li-ion battery, [38] was imaged by x-ray nano-tomography [39]. Second, two lanthanum strontium manganite–yttria-stabilized zirconia (LSM–YSZ), SOFC cathodes, with LSM:YSZ weight ratios of = 70:30 (70/30) and 50:50 (50/50), were imaged and reconstructed using focused ion beam-scanning electron microscopy (FIB-SEM) serial sectioning [29]. Both the geometrical method and effective diffusion methods were applied to calculate the tortuosities of these 3D structures. The following phases were in the interest: the electrolyte (pore) phase in $LiCoO_2$, and the pore and YSZ phases in the LSM–YSZ.

The detailed description for the effective diffusion method can be found elsewhere [22]. The geometrical method used here to calculate tortuosity was based on directional distance map propagation. As it is important to calculate tortuosity along different directions in the microstructure to reveal the anisotropy [32], the tortuosity was calculated in three orthogonal directions (x, y and z). Within the phase of interest, only the interconnected portions that can contribute to transport were included in the calculation.

Here we elaborate the details of the algorithm by describing the steps to calculate the tortuosity along the x direction. The tortuosity along two other orthogonal directions y and z were calculated using the same procedure. First, all of the phase of interest located in the starting plane, 'seed plane', are labeled with distance of unity. Second, the neighboring voxels of the phase of interest are labeled with their effective distance, and this procedure is repeated directionally through the phase network until all the voxels is labeled with a

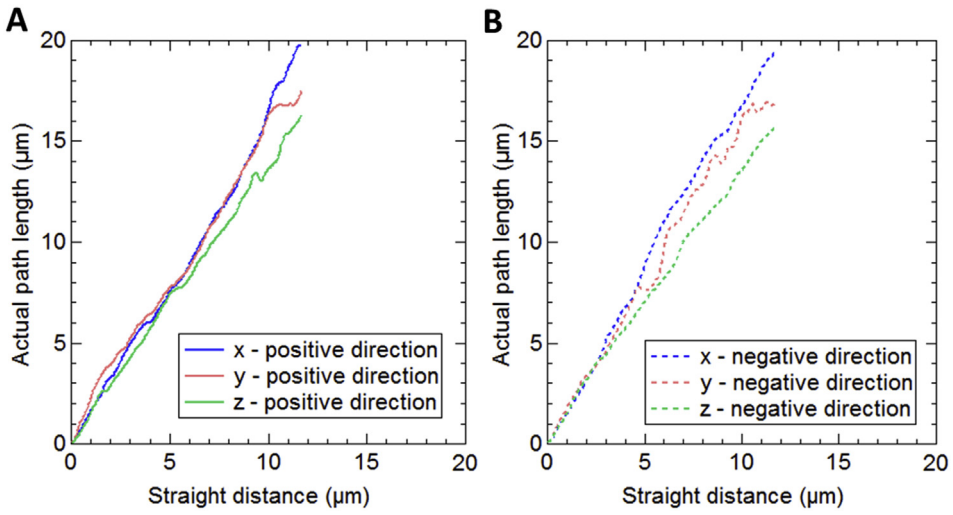

Fig. 5. Distance curves of $LiCoO_2$ show the actual path length vs. straight-through distance for all three orthogonal directions, prorogating from (A) positive and (B) negative directions.

distance. Depending on the neighboring voxel definition, the effective distance may vary. Here we adapted three different neighboring definitions: 1) city block, 2) quasi-Euclidean and 3) chess board. A schematic is shown in Fig. 1 to illustrate the concept of different neighboring definitions and how it affects the distance propagation. Third, the so-called 'distance curve', *i.e.*, a plot of the effective lengths versus the straight-through distance was obtained.

Finally, the tortuosity was calculated from the distance curve. We implemented four different methods to extract the tortuosity. The first method is by fitting the curve with one single slope as used previously in the literature [31]. Two problems arise from defining a single fitted slope as tortuosity. First, there is a possibility to obtain a slope of less than unity, which is physically impossible as an actual path cannot be less than the straight distance. Secondly, it only represents an overall trend and the step-determining slow diffusion structures are not reflected in the result. To resolve these problems, three more methods are proposed and tested here. The illustration of the different methods to extract tortuosity from the distance curve is shown in Fig. 2. Other methods are named with End, Average and Slope.

Although our method is based upon the distance propagation, we have modified it in the following aspects. First, the distance propagation was performed with the entire volume instead of from the center. As previously used in the literature, the seed plane is defined as the center plane of the sample and therefore the algorithm effectively measures two sub-volumes, which is different from measuring from the entire volume. Here, the distance propagation is performed separately along the positive and negative directions and then the average is also calculated. Secondly, we included quasi-Euclidean distance to improve the accuracy in measuring the distance between voxels. Previously by using city-block definition, the tortuosity tends to be over-estimated and by using chess-board definition, the tortuosity tends to be under-estimated. Last, different methods were used to extract the tortuosity instead of only using a single slope as its limitation pointed out previously.

With the distance map obtained via distance propagation, the following distributions can also be obtained directly: 1) histogram of tortuosity at a given plane and 2) spatial distribution of the tortuosity, viewed as a tortuosity map. This additional information provides a comprehensive picture to characterize the tortuosity and to facilitate the understanding of the transport phenomena in the porous media.

3. Results and discussion

3.1. Propagation of distance map

The reconstructed 3D microstructures of the $LiCoO_2$ and LSM–YSZ electrodes are shown in Fig. 3. Fig. 4 shows the 3D distance

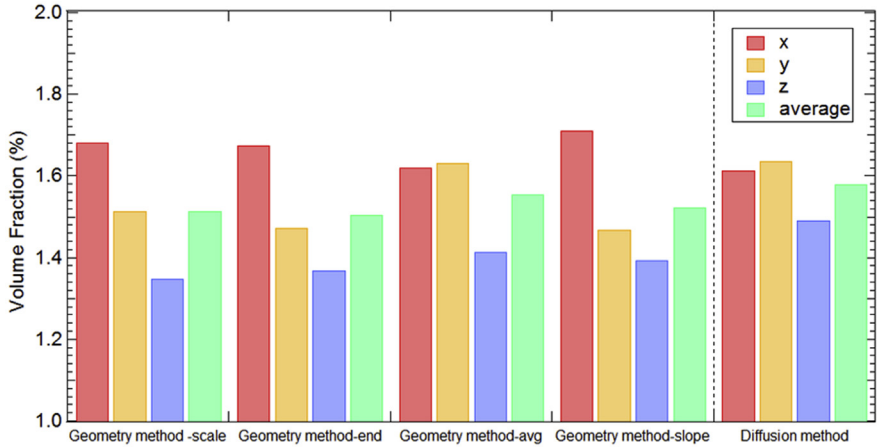

Fig. 6. Comparison of the geometry method vs. diffusion method for $LiCoO_2$ pore phase. The geometry method here used the city-block as the neighboring definition.

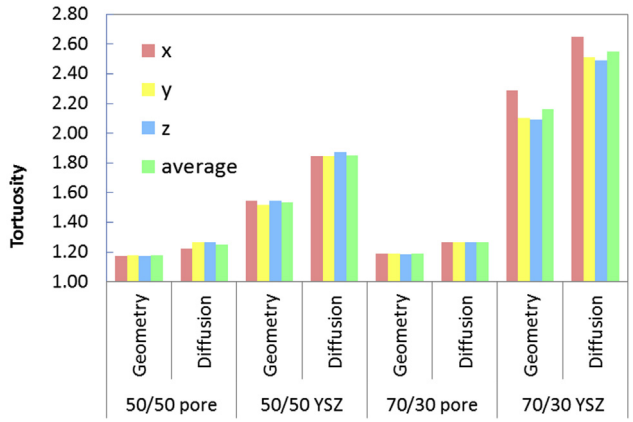

Fig. 7. Comparison of the geometry method vs. diffusion method for LSM–YSZ pore and YSZ phases, both 70/30 and 50/50 samples. The geometry method here using city-block as the neighboring definition and average as the calculation method.

maps based on geometric distance prorogation along the pores of $LiCoO_2$ for all three orthogonal directions. For each direction, the path distance maps along both positive and negative directions were calculated. For instance, Fig. 4(A, B) shows the distance propagation along the positive and negative direction of the *x* axis respectively. The similar distance maps were also obtained for the *y* and *z* directions but only the distance maps along the positive directions are shown here for brevity. The distance maps were also obtained for the LSM–YSZ sample and are not shown here for brevity.

After establishing the distance map, the average actual path length at each plane for a fixed straight distance along *x*, *y* and *z* can then be obtained. The results using the city-block neighboring definition are shown in Fig. 5. Similarly, the distance curve for the other two voxel neighboring definitions were also calculated but are not shown here for brevity.

3.2. Comparison between the geometry method and the diffusion method

The comparison of the geometrical and effective diffusion method results for $LiCoO_2$ is shown in Fig. 6. The geometry method shown here is using the city-block method as the neighboring definition, which is found to be closest to the tortuosity values calculated from the diffusion method. The effects of the neighboring definitions are discussed in Section 3.3. Among the four different definitions to extract the tortuosity in the geometry method, the definition that produced the results closest to the diffusion method was the average method. This indicates that the diffusion method has a similar nature as the geometry method when taking into account the effect of each of the individual planes and defining the total tortuosity as the average of the tortuosity from each plane.

The tortuosity results of the LSM–YSZ samples from both the geometry and diffusion methods are shown in Fig. 7. These two methods show good agreement overall with the trend when comparing the tortuosity between different phases or between different directions. For the pore phase where the tortuosity is lower, these two methods show better agreement in their values.

3.3. Effects of different parameters in the geometry method

As shown previously, the four different methods to calculate tortuosity from the distance curve lead to slightly different tortuosity results since they show different aspects when representing tortuosity. In addition to this parameter, other parameters that might affect the calculations include: distance propagation direction, sampling volume size, and neighboring voxel definition, which are discussed in the following.

For a structure that is fully connected in 3D, meaning that the distance propagation can be performed completely from both positive and negative directions, the difference that results from the direction definition is generally less than 2%, independent of other factors such as the neighboring voxel definition and also of the sampling volume size.

The sampling volume size affects the tortuosity simply due to the inhomogeneity in the studied media. Figure 8(A) shows the relationship between the tortuosity of the pores versus the sample volume size for the $LiCoO_2$ sample. The variation of the tortuosity as a function of the sampling volume is therefore an indication of the inhomogeneity of the sample.

The neighboring voxel definition affects the tortuosity in the calculation of the actual path length. A comparison between the three different neighboring definitions is shown in Fig. 8(B). By varying the neighboring voxel definition, the physical connectivity between two nearby voxels varies. It is natural that the most strict neighboring definition city-block results in the largest tortuosity since only the face-adjunct voxels are considered neighbors. It follows by the results from quasi-Euclidean which is a more neutral

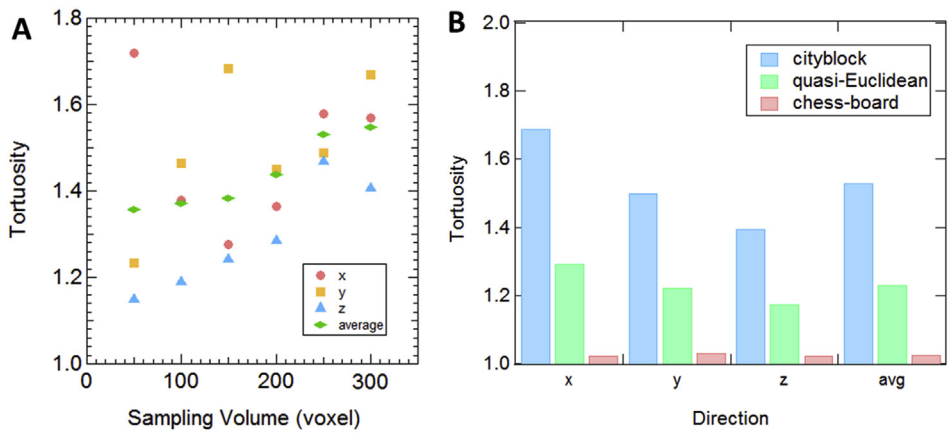

Fig. 8. (A) Tortuosity vs. sampling volume size for $LiCoO_2$ sample. Here the sampling volume is the length of the cubic volume that is being sampled. Here the sampling volume is the length of the cubic volume that is being sampled. For instance, the label 100 refers to a volume with 100 × 100 × 100 voxels. (B) The tortuosity results depend on the voxel neighboring definition – city-block, quasi-Euclidean and chess-board.

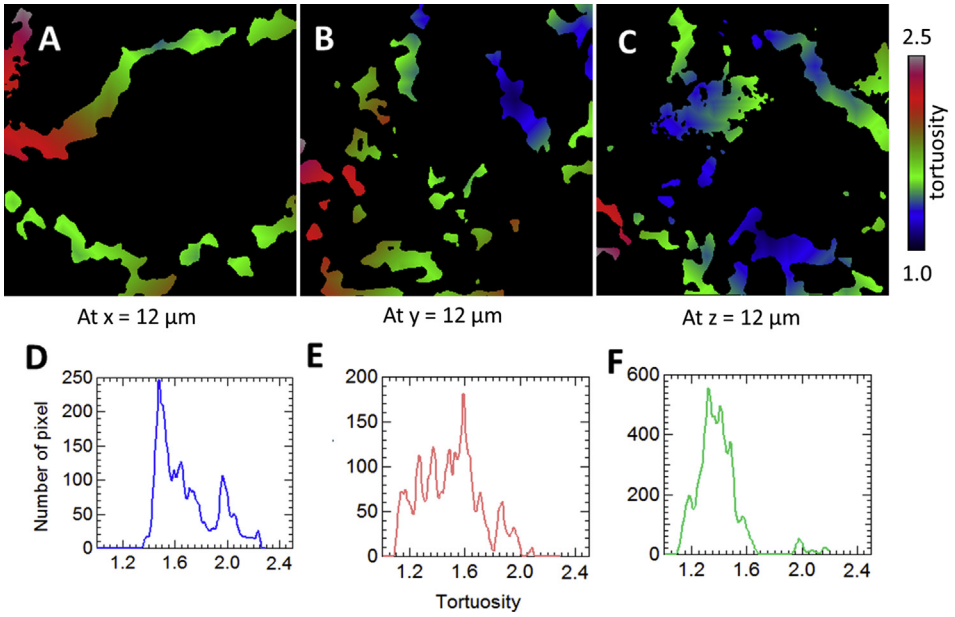

Fig. 9. "Tortuosity distribution" of the $LiCoO_2$ sample shown as (A–C) spatial distribution maps and also (D–F) histograms for all three orthogonal directions along the positive direction.

definition of the neighboring voxel distance. The chess-board definition is found to tend to underestimate the tortuosity significantly and should not be used.

3.4. Tortuosity distribution characterized by spatial distribution map and histogram

In order to overcome the limitation of using one single tortuosity value to represent the whole structure, the "tortuosity distribution" both as a spatial distribution map and also a histogram can be obtained from the distance propagation map shown in Fig. 4. The tortuosity distribution shown as spatial distribution maps for all three orthogonal directions of $LiCoO_2$ pore phase are presented in Fig. 9(A–C). The significant variation can be observed clearly with some regions of the structure has tortuosity as high as almost 2.5 and other regions of the structure as low as almost unity. This spatial variation was lost when averaging the distance along a specific distance plane and cannot be characterized by using one single tortuosity value. This tortuosity variation can also be characterized by histograms as shown in Fig. 9(D–F). A single value tortuosity only shows the mean value of the tortuosity distribution.

4. Conclusions

A geometrical tortuosity calculation method was tested on three measured 3D structures: a $LiCoO_2$ battery electrode and two 3D LSM–YSZ structures. The comparison between the geometrical and diffusivity methods was discussed, and the specific geometrical method yielding the best agreement was identified. The method and the concept of tortuosity distribution based on large volume of 3D structure using x-ray nano-tomography opens up a way of accurate and efficient characterization of the tortuosity. Although the present examples are energy materials, the method is broadly applicable to any porous or multi-phase media studies. The effective diffusivity can be derived for a given species in a given media, once the tortuosity is known. The tortuosity can also be used as a critical parameter in modeling and designing of energy storage and conversion materials.

Acknowledgments

We are grateful that Prof. Eric Maire provided us with the methodology developed by his group. We thank William Harris and Prof. Wilson Chiu for the helpful discussion. We thank Dr. Fernando Camino for assisting the development of the sample preparation procedure using FIB-SEM. Research carried out in part at the Center for Functional Nanomaterials, Brookhaven National Laboratory, which is supported by the U.S. Department of Energy, Office of Basic Energy Sciences, under Contract No. DE-AC02-98CH10886. Use of the National Synchrotron Light Source, Brookhaven National Laboratory, was supported by the U.S. Department of Energy, Office of Science, Office of Basic Energy Sciences, under Contract No. DE-AC02-98CH10886. Scott Barnett and Katsuyo Thornton gratefully acknowledge support by the National Science Foundation under Grant Number DMR-0907639/0907030.

References

[1] C.J. Bae, C.K. Erdonmez, J.W. Halloran, Y.M. Chiang, Adv. Mater. 25 (2013) 1254–1258.
[2] N.A. Zacharias, D.R. Nevers, C. Skelton, K. Knackstedt, D.E. Stephenson, D.R. Wheeler, J. Electrochem. Soc. 160 (2013) A306–A311.
[3] A. Cecen, E.A. Wargo, A.C. Hanna, D.M. Turner, S.R. Kalidindi, E.C. Kumbur, J. Electrochem. Soc. 159 (2012) B299–B307.
[4] C.L. Tsai, V.H. Schmidt, J. Power Sources 196 (2011) 692–699.
[5] A. Stein, B.E. Wilson, S.G. Rudisill, Chem. Soc. Rev. 42 (2013) 2763–2803.
[6] S. Prachayawarakorn, R. Mann, Catal. Today 128 (2007) 88–99.
[7] H.Y. Chou, L.S. Wu, L.Z. Zeng, A. Chang, Water Resour. Res. 48 (2012) 11.
[8] Z.F. Zhang, A.L. Ward, G.W. Gee, Vadose Zone J. 2 (2003) 313–321.
[9] P. Moldrup, T. Olesen, T. Komatsu, P. Schjonning, D.E. Rolston, Soil Sci. Soc. Am. J. 65 (2001) 613–623.
[10] D. Kehrwald, P.R. Shearing, N.P. Brandon, P.K. Sinha, S.J. Harris, J. Electrochem. Soc. 158 (2011) A1393–A1399.
[11] P.R. Shearing, L.E. Howard, P.S. Jorgensen, N.P. Brandon, S.J. Harris, Electrochem. Commun. 12 (2010) 374–377.
[12] I.V. Thorat, D.E. Stephenson, N.A. Zacharias, K. Zaghib, J.N. Harb, D.R. Wheeler, J. Power Sources 188 (2009) 592–600.
[13] T. Hutzenlaub, A. Asthana, J. Becker, D.R. Wheeler, R. Zengerle, S. Thiele, Electrochem. Commun. 27 (2013) 77–80.
[14] B. Vijayaraghavan, D.R. Ely, Y.M. Chiang, R. Garcia-Garcia, R.E. Garcia, J. Electrochem. Soc. 159 (2012) A548–A552.
[15] Y.C.K. Chen-Wiegart, Z. Liu, K.T. Faber, S.A. Barnett, J. Wang, Electrochem. Commun. 28 (2013) 127–130.

[16] Z. Liu, J.S. Cronin, Y.C.K. Chen-Wiegart, J.R. Wilson, K.J. Yakal-Kremski, J. Wang, et al., J. Power Sources 227 (2013) 267–274.
[17] Y.C.K. Chen-Wiegart, P. Shearing, Q.X. Yuan, A. Tkachuk, J. Wang, Electrochem. Commun. 21 (2012) 58–61.
[18] M. Doyle, J. Newman, J. Appl. Electrochem. 27 (1997) 846–856.
[19] P.A. Johns, M.R. Roberts, Y. Wakizaka, J.H. Sanders, J.R. Owen, Electrochem. Commun. 11 (2009) 2089–2092.
[20] G.M. Goldin, A.M. Colclasure, A.H. Wiedemann, R.J. Kee, Electrochim Acta 64 (2012) 118–129.
[21] P.R. Shearing, N.P. Brandon, J. Gelb, R. Bradley, P.J. Withers, A.J. Marquis, et al., J. Electrochem. Soc. 159 (2012) A1023–1027.
[22] J.R. Wilson, W. Kobsiriphat, R. Mendoza, H.Y. Chen, J.M. Hiller, D.J. Miller, et al., Nat. Mater. 5 (2006) 541–544.
[23] P. Asinari, M.C. Quaglia, M.R. von Spakovsky, B.V. Kasula, J. Power Sources 170 (2007) 359–375.
[24] J. Laurencin, R. Quey, G. Delette, H. Suhonen, P. Cloetens, P. Bleuet, J. Power Sources 198 (2012) 182–189.
[25] V.H. Schmidt, C.L. Tsai, J. Power Sources 180 (2008) 253–264.
[26] J.S. Cronin, Y.C.K. Chen-Wiegart, J. Wang, S.A. Barnett, J. Power Sources 233 (2013) 174–179.
[27] Y.C.K. Chen-Wiegart, J.S. Cronin, Q.X. Yuan, K.J. Yakal-Kremski, S.A. Barnett, J. Wang, J. Power Sources 218 (2012) 348–351.
[28] J.R. Wilson, S.A. Barnett, Electrochem. Solid State Lett. 11 (2008) B181–185.
[29] J.R. Wilson, J.S. Cronin, A.T. Duong, S. Rukes, H.Y. Chen, K. Thornton, et al., J. Power Sources 195 (2010) 1829–1840.
[30] Y. Nakashima, S. Kamiya, J. Nucl. Sci. Technol. 44 (2007) 1233–1247.
[31] E. Maire, P. Colombo, J. Adrien, L. Babout, L. Biasetto, J. Eur. Ceram. Soc. 27 (2007) 1973–1981.
[32] E. Maire, O. Caty, A. King, J. Adrien, in: Iutam Symposium on Mechanical Properties of Cellular Materials, 12, 2009, pp. 35–42.
[33] Z. Fishman, A. Bazylak, J. Electrochem. Soc. 158 (2011). B247-B252.
[34] S. Haussener, P. Coray, W. Lipinski, P. Wyss, A. Steinfeld, J. Heat Transfer Trans. Asme 132 (2010).
[35] W.B. Lindquist, S.M. Lee, D.A. Coker, K.W. Jones, P. Spanne, J. Geophys. Res. Solid Earth 101 (1996) 8297–8310.
[36] M. Axelsson, S. Svensson, Pattern Anal. Appl. 13 (2010) 159–172.
[37] N. Epstein, Chem. Eng. Sci. 44 (1989) 777–779.
[38] W. Lai, C.K. Erdonmez, T.F. Marinis, C.K. Bjune, N.J. Dudney, F. Xu, et al., Adv. Mater. 22 (2010) E139.
[39] J. Wang, Y.-c.K. Chen, Q. Yuan, A. Tkachuk, C. Erdonmez, B. Hornberger, et al., Appl. Phys. Lett. 100 (2012) 143107, 1-4.